Journal of Organometallic Chemistry 879 (2019) 27–39

Contents lists available at ScienceDirect

Journal of Organometallic Chemistry

journal homepage: www.elsevier.com/locate/jorganchem

Synthesis, characterization, crystal structures, Hirshfeld surface analysis and theoretical calculations of some new bisphosphoramidate derivatives and novel binuclear triorganotin(IV) complexes with diphosphoryl ligand

Khodayar Gholivand [a, *], Masoumeh Azadbakht [a], Yazdan Maghsoud [a], Mahdieh Hosseini [a], Canan Kazak [b]

[a] Department of Chemistry, Faculty of Science, Tarbiat Modares University, Tehran, Iran
[b] Department of Physics, Faculty of Art and Science, Ondokuz Mayıs University, Samsun, Turkey

ARTICLE INFO

Article history:
Received 14 August 2018
Received in revised form
14 October 2018
Accepted 17 October 2018
Available online 22 October 2018

Keywords:
Triorganotin(IV)
Bisphosphoramidate
Crystal structure
Hirshfeld surfaces
Theoretical studies

ABSTRACT

A series of new bisphosphoramidate and (thio)phosphoramidate derivatives with the general formula $R_1R_2P(X)-Y-P(X)R_1R_2$ have been synthesized and characterized by IR and NMR spectroscopies (**L_1**–**L_{12}**). The crystal structure of compound 1,4-[$(C_2H_5O)_2P(S)(CH_2)_3NH]_2C_4H_8N_2$ (**L_4**) is also investigated by X-ray diffraction analysis. Two novel organotin(IV) complexes μ-{1,4-[$(C_6H_5)_2P(O)(CH_2)_3NH]_2C_4H_8N_2$}[$SnR_3Cl]_2$, R_3SnCl (R = phenyl/butyl), **C_1** and **C_2**, respectively, are prepared by the reaction of new diphosphoryl ligand **L_1** and R_3SnCl under different conditions. **C_1** and **C_2** are characterized by IR and NMR spectroscopies and X-ray crystallography diffraction analysis. X-ray analysis illustrates that both complexes have similar structures containing binuclear triorganotin(IV) skeletons and ligand coordinates in a bridging mode through two phosphoryl groups. Sn(IV) coordination geometries are distorted trigonal bipyramidal (TBP) for **C_1**, and **C_2** structures contained binuclear arrangement with two $SnPh_3Cl/SnBu_3Cl$ groups linked via the bridging diphosphoryl ligand. The organization of the crystal structures and the intermolecular interactions are discussed. Hirshfeld surfaces and two-dimensional fingerprint plots are used to study short intermolecular contacts in **C_1**, **C_2**, and **L_4**. Finally, the influence of chain length and the effects of various substituents on P=O and P=S bond strength in synthesized ligands (**L_1**–**L_{12}**) and optimized ligands (**L_{13}**–**L_{17}**) are theoretically investigated by NBO analysis to survey the character of mentioned bonds in these ligands. The AIM analysis is also used to determine the nature of the P=O bond in **L_1** and also P=O and $O\cdots Sn^{4+}$ bonds in **C_1** and **C_2**. Results show ionic character for $O\cdots Sn^{4+}$ interaction in both complexes and mostly electrostatic character for P=O bond in the free ligand, but with a little shift to the covalent character after the complexation.

1. Introduction

Nowadays, considerable interest has been paid to the research on phosphoramide derivatives because of their valuable and widely applicable properties such as anticancer prodrugs [1–4], antiviral agents [5–7] and biocidal activity [8,9]. These compounds are also well-known inhibitors of various enzymes, including urease and acetylcholinesterase [10,11]. The ability of phosphoramides to coordinate to the metal atoms and form coordination compounds is also distinguished, and there are many studies on their structures [12–16].

Tin compounds play an essential role in inorganic and organometallic chemistry [17,18]. Investigations on the tin(IV) adducts continue to provide fundamental information about both the Lewis acid-base model and the reactivity of tin(IV) species [19–21]. Recently organotin(IV) compounds have received considerable attention because of their biological properties [22], particularly antitumor [23–28], antibacterial [29–32] and antifungal activity [33–35]. In addition to their biological activity, the organotin(IV) complexes have also found some applications in catalysis [36] and nonlinear optics [21,37].

* Corresponding author.
E-mail address: gholi_kh@modares.ac.ir (K. Gholivand).

https://doi.org/10.1016/j.jorganchem.2018.10.012
0022-328X/

Phosphoryl-containing compounds have been widely used as active complexation agents in organotin coordination chemistry [38]. Synthesis of di- and tri-organotin complexes, containing Sn–O bonds are growing fast [39–41], and the presence of both organotin (IV) and phosphorus moieties in a single molecular can produce a still more powerful and lasting useful complex [42,43].

In the present study, some novel bisphosphoramidate and thiophosphoramidate derivatives with the general formula $R_1R_2P(X)$-Y–$P(X)R_1R_2$, (X = O and S; Y= NH–$(CH_2)_3$–N–$(CH_2)_4$–N–$(CH_2)_3$–NH and N–$(CH_2)_4$–N–$(CH_2)_2$–NH; R_1 & R_2= (C_6H_5, OC_6H_5, NHC_6H_5, OCH_3, OC_2H_5, $NH(CO)C_6H_5$, $NH(CO)CCl_3$) (**L_1**–**L_{12}**), were synthesized and characterized by ^1H, ^{31}P NMR and IR spectroscopy. The synthesis and spectroscopic characterization (^1H, ^{31}P NMR, and IR) of two new organotin complexes, obtained from the reaction of R_3SnCl (R = phenyl/butyl) with Ph2P(O)YP(O)Ph2 ligand (Y = diamine), were also reported. The structure of the **L_4** ligand and two complexes, **C_1** and **C_2**, were determined using X-ray crystallography, which revealed the similar coordination manner of the ligand and same structure in **C_1** and **C_2** complexes. Furthermore, the crystal structures of **L_4**, **C_1**, and **C_2** and their packing systems were studied using geometrical parameters, and Hirshfeld surfaces analysis.

Moreover, NBO analysis was used to investigate the nature of P=O and P=S bonds in studied bisphosphoramidate and thiophosphoramidate ligands. The AIM analysis was also used to determine the nature of the P=O bond in **L_1** and also P=O and O···Sn^{4+} bonds in **C_1** and **C_2**.

2. Experimental

2.1. Materials and measurements

All chemicals and solvents are commercially available and were used as received without any further purification.

^1H and ^{31}P NMR spectra were recorded on a Bruker Advance DRX 500 spectrometer. ^1H chemical shifts were determined relative to internal standard TMS, and ^{31}P chemical shifts were determined relative to 85% H_3PO_4 as an external standard. Infrared (IR) spectra were recorded on a Shimadzu model IR-60 spectrometer using KBr pellets. Melting points of the compounds were obtained with an electrothermal instrument. Elemental analysis was also performed using a Heraeus CHN-O-RAPID apparatus.

2.2. General procedure for synthesis of ligands

The reagents $RPOCl_2$ (R = $C_6H_5(CO)NH$) [44], $CCl_3(CO)NH$ [45] and R_1R_2POCl (R_1 = NHC_6H_5 & R_2 = OC_6H_5, $NH(CO)C_6H_5$, $NH(CO)CCl_3$), were prepared by the reaction of aniline with $RPOCl_2$ (R = OC_6H_5, $NH(CO)C_6H_5$, $NH(CO)CCl_3$), in 2:1 M ratio. The aniline was added dropwise to a CH_3CN solution of $RPOCl_2$ at 0 °C. After eight hours stirring, the solvent was removed in vacuum, and the resulting was washed with distilled water and dried.

All Ligands except **L_4** were synthesized from the reaction of the corresponding diamine (1 mmol) in the presence of triethylamine (2 mmol) as HCl scavenger in solvent at room temperature was added dropwise to a stirred solution of RRPXCl (X = S, O) or R_1R_2POCl (2 mmol) in the same solvent at 0 °C. After 24 h stirring, the solvent was evaporated, and the residue was washed with distilled water to obtain the pure products. Ligand **L_4** was prepared by using the similar procedure but washed with THF, then the solution was filtered, and evaporation removed the solvent of the filtrate at room temperature until yellow oil product was obtained, then it was washed with n-hexane and solid product obtained. Recrystallizing of Ligand **L_4** obtained suitable crystal for X-ray diffraction from a mixture of CH_3CN/CH_3CL after the slow evaporation of the solutions at room temperature. The synthesis procedures of compounds (**L_1**–**L_{12}**) was represented in Scheme 1. Synthesis and Characterization of ligands (**L_{13}**–**L_{17}**) were reported in Ref. [46]. Physical and spectroscopic data of the new ligands are presented below:

2.2.1. 1,4-[$(C_6H_5)_2P(O)(CH_2)_3NH]_2C_4H_8N_2$ (L_1)

Powder sample; m. p: 173 °C. Anal. Calc. for $C_{34}H_{42}N_4O_2P_2$: IR data (KBr pellet, cm^{-1}): 3190 m (υ_{N-H}), 1184s ($\upsilon_{P=O}$), 723 m, 697 m (υ_{P-N}), 1115s (υ_{C-N}), 2938 m, 2806 m (υ_{aliph}). ^{31}P NMR(DMSO-d_6, ppm): δ = 21.03 m. ^1H NMR ($CDCl_3$, ppm): δ = 7.86 (m, 8H, 4Ph), 7.42 (m, 12H, 4Ph), δ = 4.95 (m, 2H, NH), δ = 3.03 (m, 4H, $2CH_2$), δ = 2.33 (m, 12H, $6CH_2$), δ = 1.69 (m, 4H, $2CH_2$).

2.2.2. 1,4-[$(C_6H_5O)_2P(O)(CH_2)_3NH]_2C_4H_8N_2$ (L_2)

Powder sample; m. p: 100 °C. Anal. Calc. for $C_{34}H_{42}N_4O_6P_2$: IR data (KBr pellet, cm^{-1}): 3239 m (υ_{N-H}), 1195s ($\upsilon_{P=O}$), 760 m (υ_{P-N}), 935s (υ_{P-O}), 1242s (υ_{C-O}), 1101s (υ_{C-N}), (2935, 2870, 2811)m ($\upsilon_{aliph.}$). ^{31}P NMR (DMSO-d_6, ppm): δ = 0.696 m. ^1H NMR ($CDCl_3$, ppm): δ = 7.33 (t, 8H, 4OPh), δ = 7.25 (d, 8H, 4OPh), δ = 7.16 (t, 4H, 4OPh), δ = 4.74 (m, 2H, NH), δ = 3.19 (m, 4H, $2CH_2$).

2.2.3. 1,4-[$(C_6H_5O)(C_6H_5NH)P(O)(CH_2)_3NH]_2C_4H_8N_2$ (L_3)

Powder sample; m. p:106 °C. Anal. Calc. for $C_{34}H_{44}N_6O_4P_2$: IR data (KBr pellet, cm^{-1}) 3180 m (υ_{N-H}), 1212s ($\upsilon_{P=O}$), (756, 687, 918) m (υ_{P-N}), 918 m (υ_{P-O}), 1212s (υ_{C-O}), 2940w, 2822w ($\upsilon_{aliph.}$), 1107w (υ_{P-N}), 1293w (υ_{P-O}). ^{31}P NMR (DMSO-d_6, ppm): δ = 5.261 m. ^1H NMR(DMSO-d_6, ppm): δ = 7.85 (d, 2H, $2NH_{An}$), δ = 7.35 (t, 8H, 2O-OPh+2OAn), δ = 7.143 (2d, 8H, 2m-OPh+2mAn), δ = 6.825 (t, 4H, 2p–OPh+2p-An), δ = 5.287 (m, 2H, NH), δ = 3.27 (m, 4H, $2CH_2$), δ = 2.42 (m, 12H, $6CH_2$), δ = 1.443 (m, 4H, $2CH_2$).

2.2.4. 1,4-[$(C_2H_5O)_2P(S)(CH_2)_3NH]_2C_4H_8N_2$ (L_4)

Powder sample; m. p: 110 °C. Anal. Calc. for $C_{18}H_{42}N_4O_4S_2P_2$: IR data (KBr pellet, cm^{-1}) 3083 m (υ_{N-H}), 806s ($\upsilon_{P=S}$), 608w (υ_{P-N}), 948 (υ_{P-O}), 1029 (υ_{C-O}), 1124 m (υ_{C-N}), (2937, 2824)m ($\upsilon_{aliph.}$).^{31}P NMR($CDCl_3$, ppm): δ = 71.49 m. ^1H NMR($CDCl_3$, ppm): δ = 4.53 (several m, 2H, NH), δ = 1.31 (m, 12H, 4Me, OEt), δ = 4.04 (m, 8H, $4CH_2$, OEt), δ = 3.054 (m, 4H, $2CH_2$), δ = 2.686 (m, 12H, $6CH_2$), δ = 7.70 (m,4H, $2CH_2$).

2.2.5. 1,4-[$(CH_3O)_2P(S)(CH_2)_3NH]_2C_4H_8N_2$ (L_5)

Powder sample; m. p: 112 °C. Anal. Calc. for $C_{14}H_{34}N_4O_4S_2P_2$: IR data (KBr pellet, cm^{-1}) 3079w (υ_{N-H}), 799s ($\upsilon_{P=S}$), 627 m (υ_{P-N}), 1173w (υ_{C-N}), 1035s (υ_{P-O}), 1095 m (υ_{C-O}), (2944, 2825)m (υaliph). ^{31}P NMR($CDCl_3$, ppm): δ = 75.22 m. ^1H NMR (CDCl3, ppm): δ = 4.74 (several m, 2H, NH), δ = 3.62 (s, 12H, 4Me, OMe), δ = 3.05 (m, 4H, $2CH_2$), δ = 2.33 (m, 12H, $6CH_2$), δ = 1.74 (m, 4H, $2CH_2$).

2.2.6. 1,4-[$(CCL_3(CO)NH)(C_6H_5NH)P(O)(CH_2)_3NH]_2C_4H_8N_2$ (L_6)

Powder sample; m. p: 176 °C. Anal. Calc. for $C_{26}H_{36}N_8O_4Cl_6P_2$: IR data (KBr pellet, cm^{-1}): 3303 m, 3170w (υ_{N-H}), 1621s ($\upsilon_{C=O}$), 1169s ($\upsilon_{P=O}$), 1287s,1327s (υ_{C-N}), 920s, 748 m, 685s (υ_{P-N}), 491 m (υ_{C-Cl}), 2821 m ($\upsilon_{aliph.}$). ^{31}P NMR (DMSO-d_6, ppm): δ = −1.244 m. ^1H NMR (DMSO-d_6, ppm): δ = 7.68 (m, 2H, An), δ = 6.64–7.60 (m, HAr), δ = 3.15 (m, 4H, $2CH_2$), δ = 2.423 (m, 12H, $6CH_2$), δ = 1.677 (m, 4H, $2CH_2$). δ = 8.3 (m, 2H, $2NH_{Amide}$).

2.2.7. 1,4-[$(C_6H_5(CO)NH)(C_6H_5NH)P(O)(CH_2)_3NH]_2C_4H_8N_2$ (L_7)

Powder sample; m. p: 175–180 °C. Anal. Calc. for $C_{36}H_{46}N_8O_4P_2$: IR data (KBr pellet, cm^{-1}). 3300s, 3165s (υ_{N-H}), 1661s ($\upsilon_{C=O}$), 1202s ($\upsilon_{P=O}$), 1099 m (υ_{C-N}), (1099, 950, 694)m (υ_{P-N}), 2923w, 2807 m ($\upsilon_{aliph.}$). ^{31}P NMR (DMSO-d_6, ppm): δ = 1.833 m, ^1H NMR (DMSO-d_6, ppm):δ = 9.5 (m, 2H, $2NH_{Amide}$), δ = 7.855 (m, 2H, An), δ = 4.77 (m, 2H, NH), δ = 6.754–7.602 (m, 20H, Ar), δ = 2.91 (m, 12H, $6CH_2$), δ = 2.214 (m, 4H, $2CH_2$), δ = 1.52 (m, 4H, $2CH_2$).

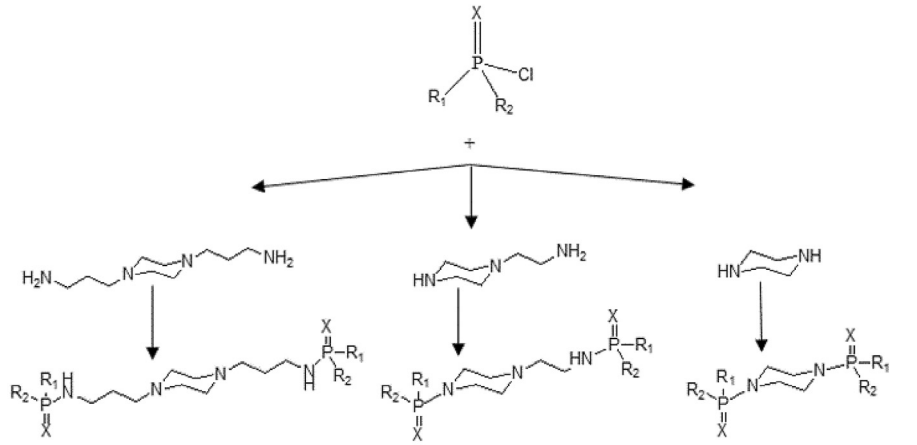

X=O, R_1=R_2=C_6H_5 (L_1) X=O, R_1=R_2=C_6H_5 (L_8) X=O, R_1=R_2=C_6H_5 (L_{13})

X=O, R_1=R_2=OC_6H_5 (L_2) X=O, R_1=R_2=OC_6H_5 (L_9) X=O, R_1=R_2=OC_6H_5 (L_{14})

X=O, R_1=NHC_6H_5, R_2=OC_6H_5 (L_3) X=O, R_1=NHC_6H_5, R_2=OC_6H_5 (L_{10}) X=O, R_1=NHC_6H_5, R_2=OC_6H_5 (L_{15})

X=S, R_1=R_2=OC_2H_5 (L_4) X=S, R_1=R_2=OC_2H_5 (L_{11}) X=S, R_1=R_2=OC_2H_5 (L_{16})

X=S, R_1=R_2=OCH_3 (L_5) X=O, R_1=$NH(CO)C_6H_5$, R_2=NHC_6H_5 (L_{12}) X=S, R_1=R_2=OCH_3 (L_{17})

X=O, R_1=NHC_6H_5, R_2=$NH(CO)CCl_3$ (L_6)

X=O, R_1=$NH(CO)C_6H_5$, R_2=NHC_6H_5 (L_7)

Scheme 1. Preparation pathway of diphosphoryl ligands.

2.2.8. 1,4-[$(C_6H_5)_2P(O)N]_2(CH_2)_2C_4H_9N$ (L_8)

Powder sample; m. p: 57 °C. Anal. Calc. for $C_{30}H_{33}N_3O_2P_2$: IR data (KBr pellet, cm^{-1}): 3208w (υ_{N-H}), 1188s ($\upsilon_{P=O}$), 1119s (υ_{C-N}), 962 m, 723s, 697s (υ_{P-N}), (3059, 2934, 2860)w ($\upsilon_{aliph.}$). ^{31}P NMR ($CDCl_3$, ppm): $\delta = 29.14$ m, 24.06 m. ^1H NMR ($CDCl_3$, ppm): $\delta = 7.83$ (m, 8H, 4Ph), $\delta = 7.42$ (m, 12H, 4Ph), $\delta = 3.72$ (m, 1H, NH), $\delta = 3.192$ (m, 6H, $3CH_2$), $\delta = 2.55$ (m, 6H, $3CH_2$).

2.2.9. 1,4-[$(C_6H_5O)_2P(O)N]_2(CH_2)_2C_4H_9N$ (L_9)

Oil sample; Anal. Calc. for $C_{30}H_{33}N_3O_6P_2$: IR data (KBr pellet, cm^{-1}): 3232w (υ_{N-H}), 1193s ($\upsilon_{P=O}$), 930s, 769 m (υ_{P-N}), 930s (υ_{P-O}), 1266 m (υ_{C-O}), (2931, 2815, 2675)w ($\upsilon_{aliph.}$). ^{31}P NMR (DMSO-d_6, ppm): $\delta = 0.749$ m, 0.625 m. ^1H NMR (DMSO-d_6, ppm): $\delta = 7.37$ (m, 8H, 4OPh), $\delta = 7.24$ (m, 12H, 4OPh), $\delta = 5.74$ (m, 1H, NH), $\delta = 3.07$ (m, 6H, $3CH_2$), $\delta = 2.23$ (m, 6H, $3CH_2$).

2.2.10. 1,4-[$(C_6H_5O)(C_6H_5NH)P(O)N]_2(CH_2)_2C_4H_9N$ (L_{10})

Powder sample; m. p: 54 °C. Anal. Calc. for $C_{30}H_{35}N_5O_4P_2$: IR data (KBr pellet, cm^{-1}) 3186 m (υ_{N-H}), 1211s ($\upsilon_{P=O}$), 1148w (υ_{C-N}), 756 m, 691w (υ_{P-N}), 924s (υ_{P-O}), 1292w (υ_{C-O}), 2967w, 2893w, 2817w ($\upsilon_{aliph.}$). ^{31}P NMR (DMSO-d_6, ppm): $\delta = 4.524$ m, 5.298 m. ^1H NMR (DMSO-d_6, ppm): $\delta = 8.05$ (m, 1H, $1NH_{An}$), $\delta = 7.87$ (m, 1H, $1NH_{An}$), $\delta = 7.28–7.395$ (2t, 8H, 2O-OPh+2O-An), $\delta = 7.04–7.16$ (2d, 8H, 2m-OPh+2m-An), $\delta = 6.81–6.89$ (2t, 4H, 2p-OPh+2p-An), $\delta = 5.1$ (m, 1H, NH), $\delta = 3.035$ (m, 6H, $3CH_2$), $\delta = 2.11$ (m, 6H, $3CH_2$).

2.2.11. 1,4-[$(C_2H_5O)_2P(S)N]_2(CH_2)_2C_4H_9N$ (L_{11})

Powder sample; m. p: 85 °C. Anal. Calc. for $C_{16}H_{33}N_3O_4S_2P_2$: IR data (KBr pellet, cm^{-1}): 3211 m (υ_{N-H}), 798s ($\upsilon_{P=S}$), 1164 m (υ_{C-O}), 1028s (υ_{C-N}), 633 m (υ_{P-N}), 957s (υ_{P-O}), (2982, 2905, 2502)w ($\upsilon_{aliph.}$). ^{31}P NMR (DMSO-d_6, ppm): $\delta = 73.2031$ m, 72.3935 m. ^1H NMR ($CDCl_3$, ppm): $\delta = 5.755$(several m, 1H, NH), $\delta = 3.93$ (m, 8H, $4CH_2$, OEt), $\delta = 1.21$ (m, 12H, 4Me, OEt), $\delta = 3.192$ (m, 6H, 3 CH_2), $\delta = 2.482$ (m, 6H, $3CH_2$).

2.2.12. 1,4-[$(C_6H_5(CO)NH)(C_6H_5NH)P(O)N]_2(CH_2)_2C_4H_9N$ (L_{12})

Powder sample; m. p: 145–150 °C. Anal. Calc. for $C_{32}H_{37}N_7O_4P_2$: IR data (KBr pellet, cm^{-1}): 3400w, 3197 m (υ_{N-H}), 1667s, 1601 m ($\upsilon_{C=O}$), 1209s, 1276 m ($\upsilon_{P=O}$), 1072 (υ_{C-N}), (1072, 975, 704) (υ_{P-N}), 2923s, 2900w ($\upsilon_{aliph.}$). ^{31}P NMR(DMSO-d_6, ppm): $\delta = 2.398$ m, 1.27, ^1H NMR (DMSO-d_6, ppm): $\delta = 9.63$ (m, 2H, $2NH_{Amide}$), $\delta = 8.8$ (m, 2H, NH), $\delta = 4.64$ (m,1H, 1NH), $\delta = 6.7–7.9$ (m, 20H, Ar), $\delta = 3.03$ (m, 6H, $3CH_2$), $\delta = 2.355$ (m, 6H, $3CH_2$).

2.3. Synthesis of metal complexes

Complex **C_1**: A solution of $Sn(Ph)_3Cl$ (2 mmol) in methanol was added dropwise to a solution of ligand **L_1** (1 mmol) in the same solvent at room temperature.

Complex **C_2**: The synthesis of **C_2** was carried out identically to **C_1**, using $Sn(Bu)_3Cl$ instead of $Sn(Ph)_3Cl$ and reaction solvent was toluene.

Suitable crystals of **C_1** and **C_2** for X-ray diffractions were obtained from slow evaporation of the clear solutions at room temperature. Physical and spectroscopic data of the synthesized complexes are presented below:

2.3.1. μ-{1,4-[$(C_6H_5)_2P(O)(CH_2)_3NH]_2C_4H_8N_2$}[$SnPh_3Cl]_2$ (C_1)

Mp: 202 °C. Anal. Calc. for $C_{70}H_{72}Cl_2N_4O_2P_2Sn_2$: IR data (KBr pellet cm^{-1}): 3053w (υ_{N-H}), 1156s ($\upsilon_{P=O}$), 730s, 693 m (υ_{P-N}), 1122s (υ_{C-N}), 2945w, 2820w ($\upsilon_{aliph.}$).^{31}P NMR(DMSO-d_6, ppm): $\delta = 21.33$ m, ^1H NMR (DMSO-d_6, ppm), $\delta = 5.32$ m (several m, 2H, NH), $\delta = 7.4–7.5$ (m, 31H, 4Ph, Ph_3Sn), $\delta = 7.75–7.79$ (m, 10H, 4Ph, Ph_3Sn), $\delta = 7.84–7.9$ (m, 9H, 4Ph, Ph_3Sn), $\delta = 3.28$ (m, 4H, $2CH_2$), $\delta = 2.77$ (m, 12H, $6CH_2$), $\delta = 1.58$ (m, 4H, $2CH_2$).

2.3.2. μ-{1,4-[$(C_6H_5)_2P(O)(CH_2)_3NH]_2C_4H_8N_2$}[$SnBu_3Cl]_2$ (C_2)

Mp: 194 °C. Anal. Calc. for $C_{58}H_{60}Cl_2N_4O_2P_2Sn_2$: IR data (KBr pellet cm^{-1}): 3063w (υ_{N-H}), 1162s ($\upsilon_{P=O}$), 731w, 694 m (υ_{P-N}), 1127s

(υ_{C-N}), 2950s, 2921s, 2854 m ($\upsilon_{aliph.}$). ^{1}P NMR (DMSO-d_6, ppm): $\delta = 21.14$ m, ^{1}H NMR(DMSO-d_6, ppm), $\delta = 5.4$ m (several m, 2H, NH), $\delta = 7.76$ (m, 8H, 4Ph), $\delta = 7.469$ (m, 12H, 4Ph), $\delta = 3.3$ (m, 4H, $2CH_2$), $\delta = 2.75$ (m, 12H, $6CH_2$), $\delta = 2.22$ (m, 4H, $2CH_2$).

2.4. Crystal structure determination

X-ray intensity data were collected at 100 K on a Bruker SMART APEXII CCD diffractometer (**L_4**), and at 0 K on an Xcalibur, Eos diffractometer (**C_1** and **C_2**) with graphite-monochromatized Mo Kα radiation ($\lambda = 0.71073$ Å). The structures were solved by direct methods using SHELXTL-2009 [47], ShelXT-2015 [48] and ShelXS-2008 [47] for **L_4**, **C_1**, and **C_2**, respectively. Then the structures were refined with the full-matrix least-squares procedure on F^2 by SHELXTL-2009 for **L_4** and ShelXT-2015 for **C_1** and **C_2**. All non-hydrogen atoms have been refined anisotropically. Hydrogen atoms have been added at calculated positions and refined using a riding model based on the parent atom. In the structure of **C2**, the butyl Ligands are disordered over two positions with 0.65/0.35 occupancies. In the crystal packing figures of this complex, the minor component of the disordered atoms is omitted for clarity. Structural artworks have been drawn with MERCURY [49]. The CIF files have been deposited with the CCDC and have been given the deposition numbers 1847678, 1847679 and 1847680 for **L_4**, **C_1**, and **C_2**, respectively.

2.5. Computational details

All of the quantum chemical computations were implemented by the use of Gaussian 03 program package [50]. Density functional theory (DFT) was utilized, which can characterize the structure of ligands and complexes quantitatively. Coulomb-attenuating method (CAM-B3LYP) was used as a hybrid exchange-correlation functional, which combines the hybrid qualities of B3LYP and the long-range correction presented by Tawada et al. [51]. All the atoms were treated by the def2-TZVP [52], basis set in H_2O and the temperature of 293 K (room temperature) using the SMD solvation model. Frequency calculations were accomplished at the same level of theory as those for the structural optimization. Vibrational frequency analysis, calculated at the same levels of theory, indicates that optimized structures are at the stationary points corresponding to local minima without any imaginary frequency. The atoms in molecules theory (AIM) analysis was carried out using AIM2000 program [53], in which the wave function was obtained from the aforementioned basis sets at the CAM-B3LYP level of theory. Natural bond orbital (NBO) analysis was performed with the NBO program, embedded in the Gaussian package. Delocalization stability energy, $\Delta E_{ij}^{(2)}$ in NBO approach is defined by the following equation:

$$\Delta E_{ij}^{(2)} = \frac{\left|\varphi_i|\widehat{F}|\varphi_j\right|^2}{\varepsilon_i - \varepsilon_j}$$

Where, $\widehat{F}$ is the Fock operator, φ_i and φ_j are the electron donor and electron acceptor orbitals respectively, and ε_i and ε_j are their corresponding energies [54].

3. Results and discussion

3.1. Spectral study

All compounds were characterized by IR and NMR spectroscopy. Relevant spectroscopic data of new bisphosphoramidate derivatives and complexes **C_1** and **C_2** are presented in supplementary data. The analysis of the IR spectra indicated that the fundamental ?(P=O) stretching modes and ?(P=S) for compounds appeared at 1169–1276 and 798–806 cm^{-1}, respectively. Other fundamental characteristics of these compounds are N–H and P–N stretching modes, appear at the values around 3079–3400 and 608–1099 cm^{-1}, respectively. Besides, a significant decreasing of the N–H stretching frequencies is observed in complexes **C_1** and **C_2**. As well the N–H bond participates in the hydrogen bonding, the positive shift of ?(N–H) may be attributed to the weakening of the hydrogen bonds from NH···$O_{p=o}$ in the free ligands to NH···Cl in its complexes. Moreover, The C=O stretching modes for **L_6**, **L_7**, and **L_{12}** compounds appear at 1601–1667 cm^{-1}.

The stretching frequencies of P=O groups in complexes **C_1** and **C_2** appear at 1156 and 1162 cm^{-1}, respectively, which are at a lower frequency concerning the related free ligand (1184 cm^{-1}). That support coordination of ligand to the metal via the oxygen atom of phosphoryl group in both complexes, which are confirmed by X-ray diffraction studies. Besides, the low-frequency shifts are higher in the complex **C_1** (including with substituents $SnPh_3Cl$) confirming that the Sn–O interaction is stronger than **C_2**.

Phosphorus chemical shift values $\delta(^{31}P)$ for compounds were observed in the range of −1.24–29.14 ppm for P=O and 71.49–75.22 ppm for P=S derivatives. As ^{31}PNMR spectra reveal, compounds with P=S group indicated a higher upfield shift in comparison to compounds with the P=O group. The ^{31}PNMR spectra for compounds indicated similar and multiplet splitting pattern; This splitting pattern arising from spin couplings between the phosphorus nucleus with NH and protons of the CH_2. ^{31}P NMR spectroscopic results indicated that chemical shift $\delta(^{31}P)$ for the complexes were also very close to the value of the related free ligand. The ^{1}H NMR spectral data obtained for ligands are indicative of the expected structure for these molecules.

The integrated ^{1}H NMR spectra in complexes **C_1** and **C_2** are in accordance with the binuclear structures, which exhibit the expected proton signals for a bridging ligand and two triphenyl and tributyltin(IV) respectively.

3.2. Single crystal X-ray diffraction studies

3.2.1. Descriptions of crystal structures

Single crystals of **L_4**, **C_1**, and **C_2** were obtained by slow evaporation of solvent at room temperature with excellent quality. Crystallographic data of mentioned compounds as well as their geometric parameters are summarized in Tables 1 and 2, respectively. Molecular structures of **L_4**, **C_1**, and **C_2** are presented in Fig. 1.

L_4 crystallizes in the triclinic crystal system with space group $P\bar{1}$. Both complexes **C_1** and **C_2** form in the monoclinic crystal system with space groups $P2_1/n$ and $P2_1/c$, respectively.

As shown in Fig. 1, the structure of **C_1** and **C_2** complexes are quite similar. X-ray analysis revealed that the asymmetric unit of these two complexes consists of one $Sn(Ph/Bu)_3$ metal center, half of the bidentate bisphosphoramidate ligand, and one coordinated chloride anion. So **C_1** and **C_2** contain binuclear arrangement with two $SnPh_3Cl/SnBu_3Cl$ groups linked via the bridging diphosphoryl ligand. The bidentate ligand has P=O groups in an anti-conformation related to each other.

The coordination polyhedra around tins can be described as slightly distorted trigonal bipyramidal with three phenyl/butyl carbon atoms occupying the equatorial positions and the chlorine atom and the phosphoryl group at the apices positions. The trans angles found around the metal are 176.38(6) (**C_1**), and 178.7(2) (**C_2**), as well as the sum of the angles subtended at tin in the trigonal girdle, is 358.4(1) and 358(1) for complexes **C_1** and **C_2**, respectively. The value of the Sn–C distances for complexes are in good agreement with published values [55] and corresponds well to the sum

Table 1
Crystal data and structural refinement for compounds **L_4**, **C_1** and **C_2**.

	L_4	C_1	C_2
Empirical formula	C18H42N4O4P2S2	C70H72Cl2N4O2P2Sn2	C58H42Cl2N4O2P2Sn2
Formula weight	504.62	1371.53	1197.17
Temperature (K)	100(2)	295(2)	100(2)
Wavelength (A)°	0.71073	0.71073	0.71073
Crystal system, space group	Triclinic, $P\bar{1}$	Monoclinic, $P2_1/n$	Monoclinic, $P2_1/c$
a/Å	7.7306(6)	9.8673(4)	10.9616(9)
b/Å	8.2289(6)	20.4833(7)	31.314(2)
c/Å	10.7584(8)	16.4063(6)	9.8585(9)
α (°)	80.5560(10)	90	90
β (°)	81.3250(10)	90.269(4)	104.461(9)
γ (°)	81.3250(10)	0	90
V (Å3)	635.09(8)	3315.9(2)	3276.7(5)
Z	1	2	2
μ (mm−1)	0.21	0.928	0.930
F(000)	272	1400.0	1196.0
Crystal size (mm^3)	0.31 × 0.18 × 0.16	0.625 × 0.345 × 0.21	0.558 × 0.354 × 0.251
θ Range for data collection (°)	θ = 1.93–30.00°	2θ = 6.24–51.362°	2θ = 6.732–51.45°
Limiting indices	h = −10 → 10	*h* = −12 → 10	*h* = −13 → 13
	k = −11 → 11	*k* = −19 → 24	*k* = −17 → 38
	l = −15 → 15	*l* = 20 → 19	*l* = −7→12
Reflections collected	13421	16287	10831
Completeness to theta	99.3	0.998	0.992
Data/restraints/parameters	3678/0/138	6263/0/374	6210/0/250
Goodness-of-fit on F^2	1.001	1.030	1.019
R_1 ($I > 2\sigma(I)$)	0.0294	0.0348	0.0851
wR_2 ($I > 2\sigma(I)$)	0.0677	0.0673	0.2125
R indices (all data)	R1 = 0.0342, wR2 = 0.0709	R1 = 0.0553, wR2 = 0.0754	R1 = 0.1719, wR2 = 0.2682
Largest diff. peak and hole (e.$Å^{-3}$)	0.648 and −0.368	0.35–0.32	0.78–0.72

Table 2
Selected bond lengths (Å) and angles (°) for the crystal structures of **L_4**, **C_1**, and **C_2**.

Compound	P-(C/O)	P-N	P=O(S)	Sn-O	Sn-Cl	Sn-C	< O-Sn-Cl	< C-Sn-C
L_4	1.588(1) 1.5907(9)	1.619(1)	1.9376(6)	–	–	–	–	–
C_1	1.795(3) 1.795(3)	1.606(3)	1.481(2)	2.299(2)	2.4882(9)	2.126(3) 2.127(3) 2.115(3)	176.38(6)	117.9(1) 116.8(1) 123.7(1) 358.4(1)
C_2	1.79(1) 1.818(9)	1.626(8)	1.460(7)	2.421(6)	2.504(3)	2.21(3) 2.16(3) 2.30(3)	178.7(2)	358(1)

of the covalent radii (2.15 Å) of Sn and C atoms [56]. The Sn-Cl bonds (2.4882 (9) in **C_1** and 2.504 (3) Å in **C_2**) are in accordance with the sum of the covalent radii of Sn and Cl atoms (2.37–2.60 Å) [57]. The Sn–O bond distances (2.299(2) (**C_1**), 2.421(6) Å (**C_2**)) are longer than the sum of the covalent bond radii of Sn and O atoms, (2.038–2.115 Å) [58] but considerably shorter than the amount of their van der Waals radii of (3.71 Å) [59]. The P=O bond length in **C_1** (1.481(2) Å) and **C_2** (1.460 (7) Å) are longer than the standard P=O bond length (1.45 Å) [60]. The lengthening of the P=O bond is described merely by the polarization of the phosphoryl group in the electrostatic field of the tin(IV) atom. This fact can be observed in lower stretching frequency of the P=O bond in the IR spectra for complexes concerning the related free ligand. The Sn–O bond shortening is also accompanied by an increase in the Sn–Cl bond length and the reverse, because of the trans influence. The P=O bond elongation is in almost linear correlation with shortening of Sn–O bonds. **C_1** has the longer P=O distance and the shorter Sn–O distance comparing to **C_2**. Moreover, The Sn-Cl bond in **C_1** is shorter than it is expected. This shortening of this bond distance can be considered as a result of the packing effects and intermolecular interactions. The phosphorus atom shows a tetrahedral configuration, the average of surrounding angles around the P atoms are (109.23, 109.466 and 109.3 Å), for ligand **L_4**, complexes **C_1** and **C_2**, respectively. All of the P–N bonds are shorter than the typical P–N single bond length (1.77 Å) [60].

3.2.2. Crystal packing

L_4: The molecular structure of this compound is shown in Fig. 1(a). Two thio-phosphoryl groups adopt the anti-conformation. In the crystal structure of **L_4**, classical hydrogen bonds which are those between N–H amide group donor and piperazine nitrogen acceptors (N–H_{amidic}···N(C–N)) plus non-classical hydrogen bonds between sulfur atoms and methyl groups (C–H···S(P=S)) create one-dimensional hydrogen bonding chains along *b*-axis. As it is presented in Fig. 2 (a), the head to tail dimeric N–H···N hydrogen bonds accumulate centrosymmetric $R_2^2(12)$ amide-piperazine synthons. Besides the N–H_{amidic}···N(C–N) and C–H···S(P=S) hydrogen bonds together build up two $R_2^2(17)$ rings between two adjacent dithiophosphoryl units. So, there are two $R_2^2(17)$ and one $R_2^2(12)$ synthons between adjacent molecules in a chain along b-axis. The one-dimensional molecular chains are linked together in *ab*-plane by head-to-tail hydrogen bond interactions between sulfur atoms and methyl hydrogens (C4–H4A···S1) which result in $R_2^2(12)$ graph set motif. Therefore, P=S group is involved in bifurcated hydrogen bonds which participate in a $R_4^2(8)$ ring motif formed with assistance between

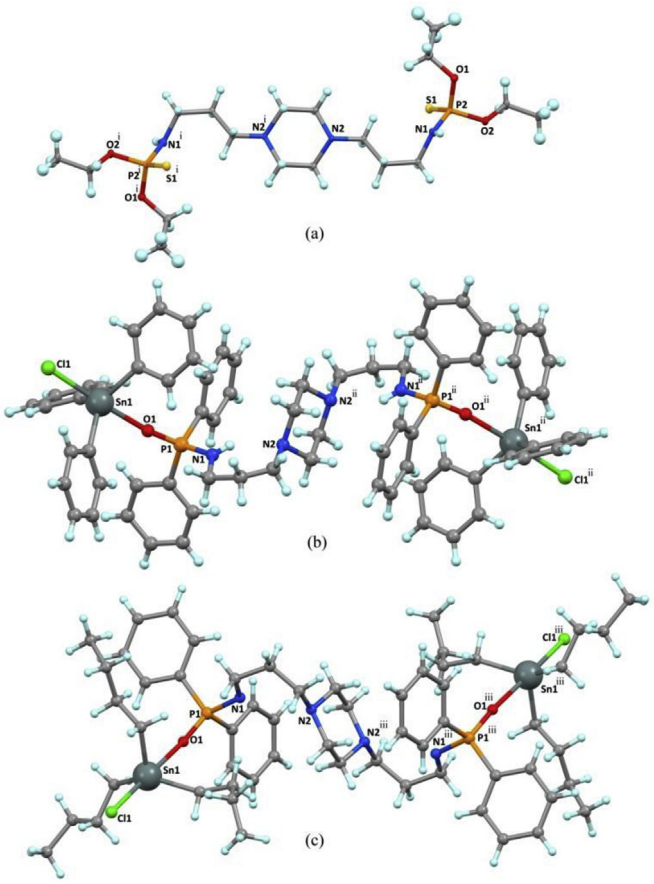

Fig. 1. Ball and stick diagram of the molecular structure of (a) $\mathbf{L_4}$; (b) $\mathbf{C_1}$ and (c) $\mathbf{C_2}$. Symmetry codes: **i**: x,2−y,1−z; **ii**: 1−x,1−y, −z; **iii**: 2−x,1−y,1−z.

four molecules of $\mathbf{L_4}$ as it is shown in Fig. 2 (b). Besides, a head to tail hydrogen bonding between the oxygen atom of diethyl group (O1) and methylic hydrogen atom (H2C) link the chain in the c-direction producing R_2^2 (8) ring motif, Fig. 2 (c). All of these intermolecular hydrogen bonds complete the whole 3D architecture of this compound in the solid state. A summary of parameters for the interactions mentioned above is presented in Tables 3 and 4.

Cg stands for the center of gravity of the mentioned ring: **For $\mathbf{C_1}$: Cg(3):** C12−C17**; Cg (4):** C18−C23; **Cg(5):** C24−C29; **Cg(6):** C30−C35; **For $\mathbf{C_2}$: Cg(2):** C1−C6; **Cg(3):** C7−C12.

$\mathbf{C_1}$: The molecular structure of this compound is shown in Fig. 1(b). In the crystal packing of this complex, the molecular units of $\mathbf{C_1}$ are joined through a C−H···π contact (C21−H21···Cg(5)) in the *a*-direction (Fig. 3(a)). The result chains are further connected to each other by two C−H···π interactions (C15−H15···Cg(3) and C32−H32···Cg(3)) in the *c*-direction (Fig. 3(b)) to generate 2D sheets in the *ac*-plane.

On the other hand, various hydrogen bonds and C−H···π contacts, including C1−H1A···Cl1, C17−H17···Cl1, C26−H26···Cg(4), C16−H16···Cg(5), C4−H4A···Cg(6) and C10−H10···Cg(5) are involved in the joining of 2D networks in the *ab*-plane which complete a 3D architecture (Fig. 4(a) and (b)). A summary of the parameters for the interactions mentioned above is presented in Tables 3 and 4

$\mathbf{C_2}$: The molecular structure of this compound is shown in Fig. 1(c). In the solid state of this binuclear complex, molecules are connected to each other by bifurcated non-classical hydrogen bonds (C14−H14A···Cl1 and C2−H2···Cl1) accompanied with a C−H···π contact (C21A−H21C···Cg(2)) which build up a chain directed along the *a*-axis (Fig. 5(a)). These chains are held together by C4−H4···Cg(2) and C4−H4···Cg(3) linkages along the *b-axis* and C10−H10···Cl1 hydrogen bonding along the c-direction, which complete a 3D network (Fig. 5b−d).

3.2.3. Hirshfeld surface analysis

Hirshfeld surface analysis is a robust technique for the quantitative study of intermolecular connections in crystal packing [61]. Consuming graphical tools based on Hirshfeld surfaces and two-dimensional (2D) fingerprint graphs to assess and relate the proportion of intermolecular associates in crystalline structures would be advantageous [62,63]. The Hirshfeld surfaces mapped with the normalized contact distance, dnorm, range 0.5−1.5 Å, and full fingerprint plots were made using the program CrystalExplorer3.0 [64], which accepts a structure input file in CIF format. The Hirshfeld surfaces of $\mathbf{L_4}$, $\mathbf{C_1}$, and $\mathbf{C_2}$ mapped with dnorm are illustrated in Fig. 6. The relative contributions of different intermolecular contacts to the Hirshfeld surface area of $\mathbf{L_4}$, $\mathbf{C_1}$, and $\mathbf{C_2}$ are shown as a chart in Fig. 7.

In the Hirshfeld surface of $\mathbf{L_4}$, the relatively large red circles specify the classic NH···N hydrogen bonds which are established between the piperazine and amine moieties. As it can be seen in the chart in Fig. 7, after H···H contact which has the most contribution in the Hirshfeld surface area, the S···H, and O···H and N···H interactions play a crucial role in the solid state of this compound.

The Hirshfeld surfaces of $\mathbf{C_1}$ and $\mathbf{C_2}$ are presented in Fig. 6. The red circles belong to Cl···H and C···H contact. In both structures after H···H contact which is dominant, with 82.6 and 66.3% for $\mathbf{C_1}$ and $\mathbf{C_2}$, respectively, the C···H interaction which is attributed to C−H···π contact, and Cl···H contact are the most significant contacts. All of these contacts between molecular components play the leading role in directing the crystal packing, while strong interaction such as H···H is anticipated not to impact on the crystallization. It is worthy to mention that the C···H contact percentage is higher in $\mathbf{C_1}$ than $\mathbf{C_2}$ because of the presence of phenyl groups in the skeleton of this complex.

3.3. Theoretical studies

Ligands studied here have the general formula $R_1R_2P(X)-Y-P(X)R_1R_2$, in which Y can be NH−$(CH_2)_3$−N−$(CH_2)_4$−N−$(CH_2)_3$−NH, NH−$(CH_2)_2$−N−$(CH_2)_4$−N, N−$(CH_2)_4$−N and connected R− groups to P=O vary as; Ph/Ph ($\mathbf{L_1}$, $\mathbf{L_8}$, $\mathbf{L_{13}}$), PhO/PhO ($\mathbf{L_2}$, $\mathbf{L_9}$, $\mathbf{L_{14}}$), PhO/PhNH ($\mathbf{L_3}$, $\mathbf{L_{10}}$, $\mathbf{L_{15}}$), PhNH/Ph(CO)NH ($\mathbf{L_7}$, $\mathbf{L_{12}}$), PhNH/Cl_3C(CO)NH ($\mathbf{L_6}$) and connected R− groups to P=S are EtO/EtO ($\mathbf{L_4}$, $\mathbf{L_{11}}$, $\mathbf{L_{16}}$) and MeO/MeO ($\mathbf{L_5}$, $\mathbf{L_{17}}$). In order to study the effectiveness of chain length and also the effects of these various substituents on phosphoramidate and thiophosphoramidate groups, which are the coordinating parts of the ligands, we have divided studied ligands ($\mathbf{L_1}$–$\mathbf{L_{17}}$) into seven different groups (Scheme 1 and Table S1). The optimized structures of all synthesized ligands and complexes at the CAM-B3LYP/def2-TZVP level of theory are represented in Fig. S1.

3.3.1. Structural parameters

P=O, P=S, and P−N calculated bond lengths in optimized free ligands are available in Table 5 (Cartesian atomic coordinates of studied structures are listed in supplementary data). Two different kinds of nitrogen may exist in the main body of ligands, which are named N_{chain} and N_{cycle}. N_{chain} is the nitrogen atom connected to the chain of carbon site, while N_{cycle} is the piperazine nitrogen atom (Scheme 2).

According to Table 5, P=O, P=S, and P−N calculated bond lengths are in the range of 1.460−1.477 Å, 1.918−1.929 Å and 1.626−1.674 Å, respectively. Among bisphosphoramidate ligands $\mathbf{L_1}$, $\mathbf{L_8}$ and $\mathbf{L_{13}}$, in which R_1 and R_2 are phenyl groups, have the most

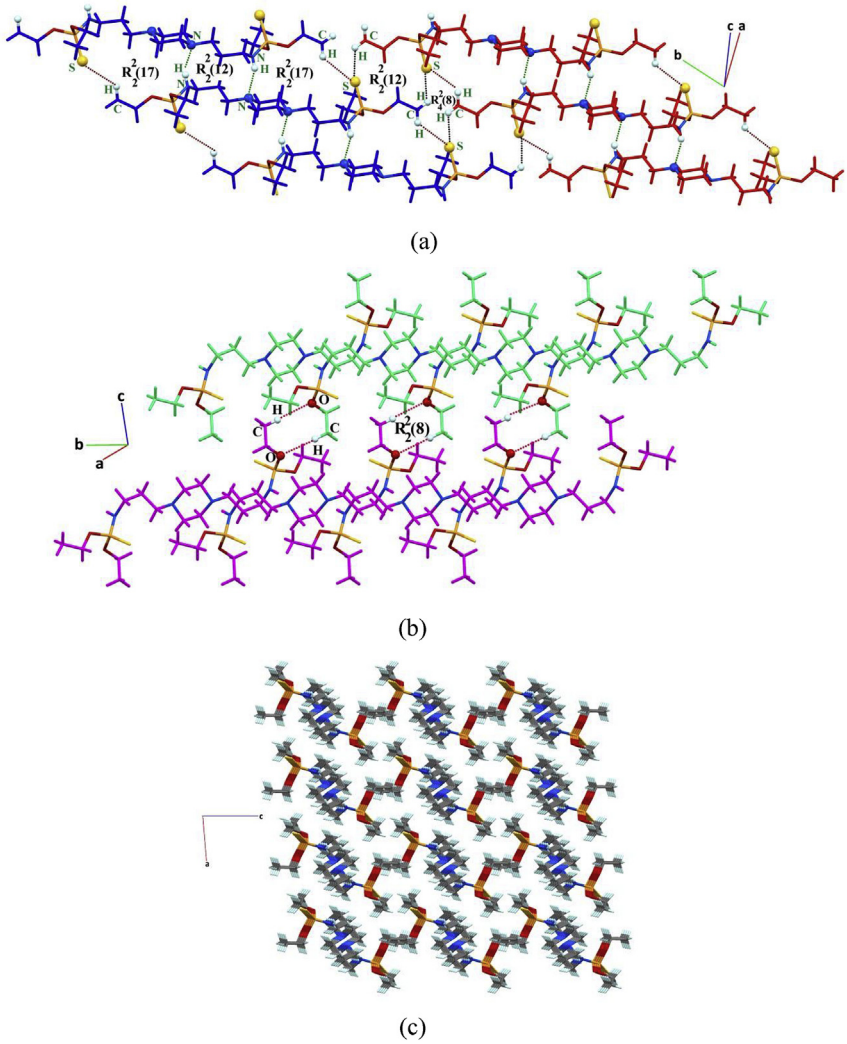

Fig. 2. Crystal packing of **L_4**: a) intermolecular hydrogen bonding linking the neighboring molecules and chains in *ab*-plane; b) head-to-tail hydrogen bonds connecting adjacent strings in *bc*-plane; c) side view of the crystal packing of **L_4** in the *ac*-plane (In (a) and (b) different colors illustrate different molecular chains). (For interpretation of the references to color in this figure legend, the reader is referred to the Web version of this article.)

Table 3
Hydrogen bond geometries for **L_4**, **C_1**, and **C_2**.

Structure	D–H	A	X-ray Geometry (Å/deg)[a]	Symmetry
L_4	C4–H4C	S1	2.993/3.731(2)/133	x,−1+y,z
	N1–H1N	N2	2.216/2.988(2)/157	−x,1−y,1−z
	C4–H4A	S1	2.999/3.716(1)/131	1−x,2−y,−z
	C2–H2C	O1	2.758/3.737(2)/179	−x,−y, 2−z
C_1	C1–H1A	Cl1	2.936/3.890(6)/160	1/2−x,1/2 + y,1/2−z
	C17–H17	Cl1	2.900/3.684(3)/143	1/2−x,1/2 + y,1/2−z
C_2	C14–H14A	Cl1	3.009/3.94(1)/162	1 + x,y,z
	C2–H2	Cl1	2.895/3.731(7)/150	1 + x,y,z
	C10–H10	Cl1	3.018/3.864(7)/152	1 + x,y,1 + z

[a] Geometrical parameters of HB-bond: H … A/D … A/<D–H … A.

extended P=O and P–N bond lengths. These parameters reach their shortest values in the case of phenoxy substituted ligands (**L_2**, **L_9**, and **L_{14}**). In all bisphosphoramidate ligands, calculated P=O bond lengths are relatively equal in both N_{cycle} and N_{chain}, while P–N bonds are longer in N_{cycle} than N_{chain}. Obtained values also demonstrate that the length of the chain (e.g., between **L_1**, **L_8**, and **L_{13}**) has a negligible effect on P=O bond lengths.

In bisthiophosphoramidate, calculated P=S and P–N bond lengths in **L_4**, **L_{11}**, and **L_{16}**, in which R_1 and R_2 are ethoxy groups, are a bit longer than that in methoxy substituted ligands (**L_5** and **L_{17}**). Both ethoxy and methoxy electron donating groups elongate the P=S and P–N bond lengths, but the effect in N_{cycle} site is more than that in N_{chain}. Overall, the length of the chain does not make any tangible change in P=O/P=S and P–N bond lengths.

3.3.2. NBO analysis

Investigation on phosphorus interaction with oxygen and sulfur have been done by NBO analysis to survey the character of mentioned bonds, which is an essential factor in coordination behavior of these ligands to a metal cation.

3.3.2.1. Bond hybridization. The hybridization of P, O, and S in related P=O and P=S bonds are illustrated in Table 6. In the case of bisphosphoramidates, the *p* character of O decreases slightly from Ph/Ph substituted ligands ($\approx sp^{1.60}d^{0.02}$) to PhO/PhNH ($\approx sp^{1.55}d^{0.02}$) and PhO/PhO ones ($\approx sp^{1.51}d^{0.02}$). The *p* character of the phosphorus atom in **L_2**, **L_9**, **L_{14}** and **L_3**, **L_{10}**, **L_{15}** ligands is also considerably smaller in comparison with other ligands. These two facts attest that the bond between P and O in these ligands is

Table 4
C–H···π interaction Geometries for $\mathbf{C_1}$ and $\mathbf{C_2}$.

Structure	Interaction/CH	CgI	X-ray Geometry (Å/deg)*	Symmetry
$\mathbf{C_1}$	C21–H21	Cg(5)	3.936/127	−1+x,y,z
	C15–H15	Cg(3)	3.980/130	−x,1−y,1−z
	C32–H32	Cg(3)	3.624/135	1−x,1−y,1−z
	C26–H26	Cg(4)	3.329/140	1/2 + x,1/2−y,−1/2 + z
	C16–H16	Cg(5)	3.327/148	1/2−x,1/2 + y,1/2−z
	C4–H4A	Cg(6)	3.450/149	−1/2 + x,1/2−y,−1/2 + z
	C10–H10	Cg(5)	3.982/170	3/2−x,1/2 + y,1/2−z
$\mathbf{C_2}$	C21A–H21C	Cg(2)	3.304/162	−1+x,y,z
	C4–H4	Cg(2)	3.750/136	x,1/2−y,−1/2 + z
	C4–H4	Cg(3)	3.309/127	x,1/2−y,−1/2 + z

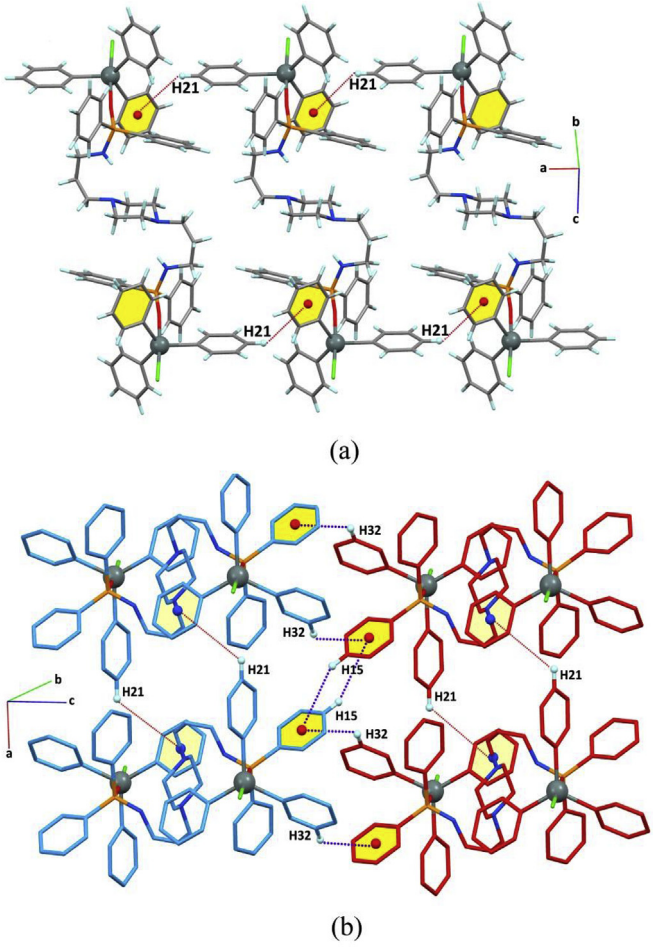

Fig. 3. Crystal packing of $\mathbf{C_1}$: (a) CH···π interaction within a chain; (b) CH···π interactions link the strings in the ac-plane. Non-interacting hydrogen atoms in (b) have been omitted for visual clarity. In (b) different colors illustrate different molecular chains. (For interpretation of the references to color in this figure legend, the reader is referred to the Web version of this article.)

stronger than the others. It is also apparent that there is not any practical difference between P=O bonds which are connected to N_{chain} or N_{cycle} and the length of the chain also doesn't make any remarkable effect on the P=O bond strength. The hybridization of P in P–N bonds demonstrate maximum and minimum *p* character in Ph/Ph and PhO/PhO substituted ligands (Table S2) which means that both kinds of P–N bonds (N_{chain} and N_{cycle}) in $\mathbf{L_1}$, $\mathbf{L_8}$, and $\mathbf{L_{13}}$ are considerably weaker in comparison to other ligands.

In bisthiophosphoramidates, the P=S bonds are composed of one sigma (σ) and one pi (π) bond. This kind of bond has an energy less than twice that of a single bond, indicating that the stability added by the π bond is less than the stability of a σ bond. This weakness is referring to significantly less overlap between the component p-orbitals due to their parallel orientation. This is in contrast to σ bonds, which form bonding orbitals directly between the nuclei of involved atoms, resulting in more great overlap and a strong σ bond. The σ-bonding hybridization of sulfur and phosphorus atoms in ($\mathbf{L_4}$, $\mathbf{L_{11}}$ and $\mathbf{L_{16}}$) show a bit more *p* character than $\mathbf{L_5}$ and $\mathbf{L_{17}}$ (see Table 6). When S is located in N_{chain} site ($\mathbf{L_4}$, $\mathbf{L_{11}}$ and $\mathbf{L_5}$) σ-bonding hybridization is about $sp^{4.24}d^{0.06}$ (average hybridization), while the hybridization is around $sp^{5.29}d^{0.09}$ in the case of N_{cycle} ($\mathbf{L_{11}}$, $\mathbf{L_{16}}$, and $\mathbf{L_{17}}$), but the hybridization of P is nearly close in both N_{chain} and N_{cycle}. The π-bonding hybridization of S and P represent the same behavior as the σ-bonding hybridization when its compared between methoxy and ethoxy ligands, but nearly different in N_{chain} and N_{cycle} sites. When S is connected to P–N_{cycle}, the hybridization is around $sp^{34.14}d^{0.24}$ (average value), while this value is precisely $sp^{1.00}d^{0.01}$ in N_{chain}. In the case of P, when it is connected to N_{chain}, hybridization is approximately $sp^{8}d^{5}$, but in N_{cycle} site hybridization is almost $sp^{99.99}d^{99.99}f^{1.3}$. By mentioned facts, the σ and π bonds would be stronger in P=S bonds connected to N_{chain} rather than N_{cycle}, because the participation percentage of *p*, *d*, and *f* (in phosphorus and sulfur) orbitals are higher in hybridization of P=S, connected to N_{cycle} rather than N_{chain}.

3.3.2.2. Wiberg bond index. Another factor in probing the bond strength is Wiberg bond index (WBI). Wiberg was initially defined for closed-shell and semi-empirical wave functions. For common chemical bonds, it's value is usually very close to formal bond order [65].

Wiberg bond indices of P–N, P=O, and P=S bonds are represented in Table 7. In bisphosphoramidate ligands, maximum WBI values of P=O and P–N bonds are obtained for $\mathbf{L_2}$, $\mathbf{L_9}$ and $\mathbf{L_{14}}$, while minimum values are related to $\mathbf{L_1}$, $\mathbf{L_8}$ and $\mathbf{L_{13}}$. The effect of the chain length is insignificant on bond orders. To some extent, WBIs of P=O bonds are the same when they are connected to N_{chain} and N_{cycle} sites, while in the case of P–N bonds, WBIs vary as $N_{chain} > N_{cycle}$.

In bisthiophosphoramidates, P=S and P–N calculated Wiberg bond indices are so close to each other, but when N_{chain} and N_{cycle} sites are comparing, both P=S and P–N bonds demonstrate greater bond orders in N_{chain} sites. As can be seen, the results of hybridization and WBI are in accordance with each other and unanimously attest that unlike P=O, P=S and P–N bonds are stronger when connected to N_{chain}.

3.3.2.3. Perturbation theory energy analysis. The next factor which can interpret the strength of the bond is charge transfer. This segment summarizes the second-order perturbative estimates of donor-acceptor (bond-anti bond) interactions. This analysis is executed by examining all possible interactions between filled (donor) Lewis-type NBOs and empty (acceptor) non-Lewis NBOs,

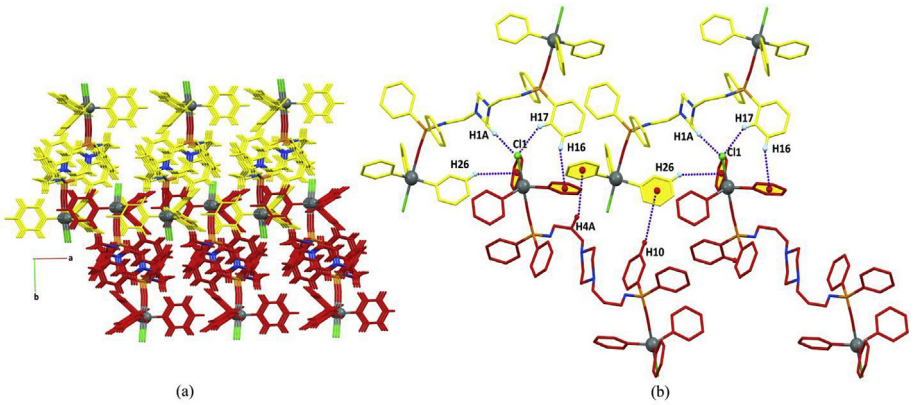

Fig. 4. Crystal packing of $\mathbf{C_1}$: (a) Three-dimensional supramolecular structure of compound $\mathbf{C_1}$; (b) The intermolecular interactions linking the adjacent 2D layers in the *ab*-plane; Non-interacting hydrogen atoms in (b) have been omitted for visual clarity; different colors present different 2D sheets. (For interpretation of the references to color in this figure legend, the reader is referred to the Web version of this article.)

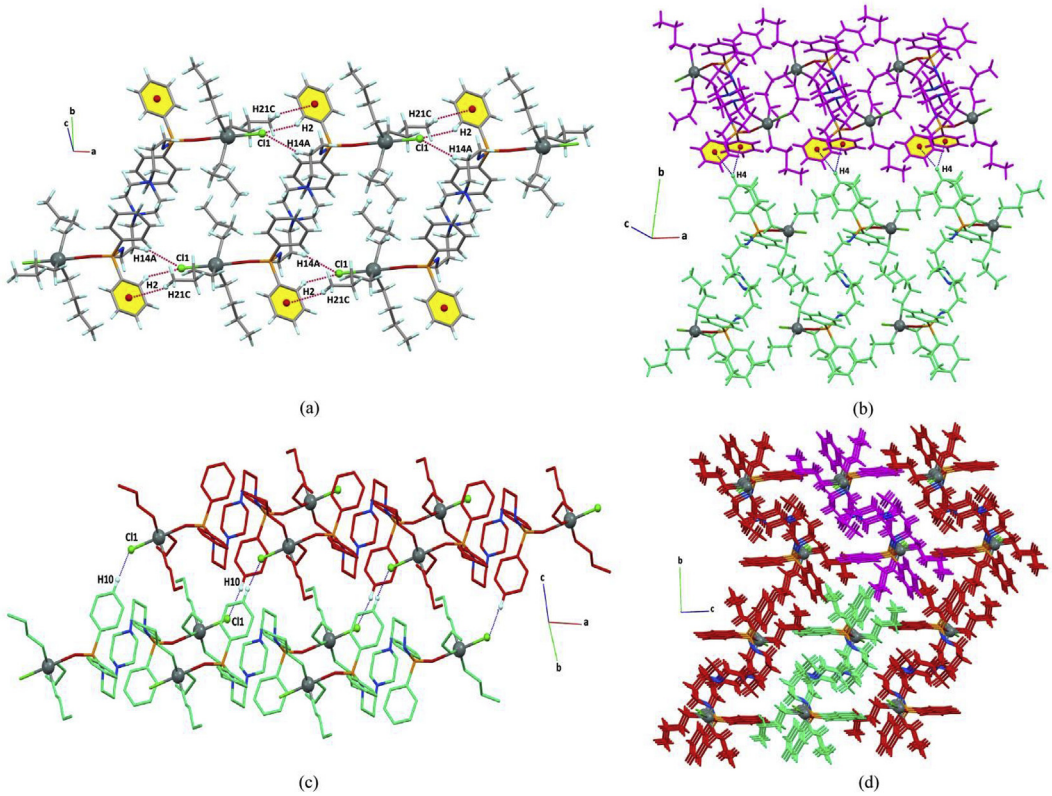

Fig. 5. Self-assembly of $\mathbf{C_2}$: (a) H-bonds and C–H···π linkages generating [100] chains; (b) C–H···π interactions which link the chains in the ab-plane; (c) Hydrogen bond connecting the strings in the ac-plane; (d) overall supramolecular array containing layers connected to each other. Non-interacting hydrogen atoms in (c) have been omitted for visual clarity. Different colors display different molecular chains. (For interpretation of the references to color in this figure legend, the reader is referred to the Web version of this article.)

and estimating their energetic importance by 2nd-order perturbation theory.

As discussed before, investigations on P=O/P=S bond lengths, bond hybridizations, and bond orders exemplified that in bisphosphoramidates, the strength of P=O bonds are relatively equal to each other when N_{chain} and N_{cycle} sites are comparing, while in bisthiophosphoramidates, P=S bonds demonstrated greater bond strength in N_{chain} sites. To authenticate mentioned results, the interactions of different atoms lone pairs with P=O/P=S antibonds ($\sigma_{P=O}^*$, $\sigma_{P=S}^*$ and $\pi_{P=S}^*$) are represented in detail in Tables S3 and S4. These data accurately explain the numerical values of the charge transfer from donor orbitals to P=O/P=S antibonds. Furthermore, total $E^{(2)}$ values from different lone pairs to $\sigma_{P=O}^*$ in Table 7 show negligible differences between N_{chain} and N_{cycle}, but charge transfers from available lone pairs to $\sigma_{P=S}^*$ and $\pi_{P=S}^*$ illustrate a considerable discrepancy among N_{chain} and N_{cycle}. Greater values of $\Delta E^{(2)}$ to P=S antibonds in N_{cycle} site attenuate the bond, while smaller values in N_{chain} site reinforce the bond.

Overall, P=O bonds in bisphosphoramidate ligands, which are involved bonds in complexation with metal cations, can be affected

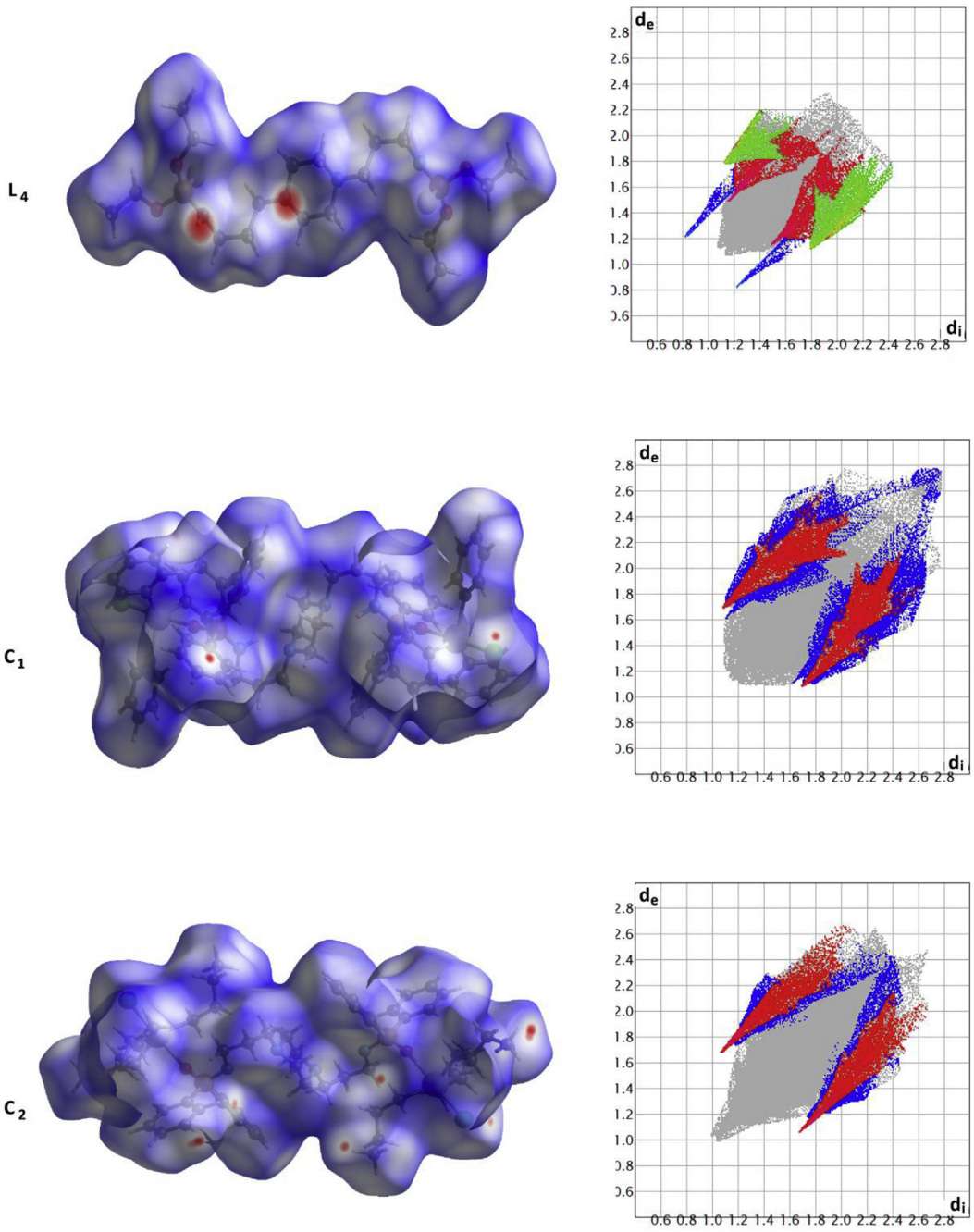

Fig. 6. Hirshfeld surfaces of **L_4**, **C_1** and **C_2** and effective interaction in 2D finger plots of compounds derived from Hirshfeld surfaces. For **L_4**, Red, blue, and green plots indicate O···H and N···H and S···H interactions, respectively. In **C_1** and **C_2**, Red and blue plots indicate Cl···H and C···H interactions, respectively. (For interpretation of the references to color in this figure legend, the reader is referred to the Web version of this article.)

by vicinal groups. This investigation illustrated that electron donating groups such as phenyl would make the P=O bond weaker, so the oxygen atom would perform a better interaction with cations by its lone pairs. P=S bonds in bisthiophosphoramidate ligands are sensitive to N_{chain} and N_{cycle} sites, and when P=S is connected to $N_{cycle,}$ the bond becomes weaker.

3.3.3. AIM analysis

The AIM analysis is an efficient tool to determine the presence of bond critical points (BCPs). The most often used criteria for the existence of covalent or ionic bonding interactions are the electron density $\rho(r)$ and the Laplacian of the electron density $\nu^2\rho(r)$ at the BCPs. The Laplacian of charge density at the BCP ($\nabla^2\rho(BCP)$) is the sum of the curvatures in the electron density along any orthogonal coordinate axes at the BCP. The sign of $\nabla^2\rho BCP$ indicates that whether the charge density is locally depleted ($\nabla^2\rho BCP > 0 > 0$) or locally concentrated ($\nabla^2\rho BCP < 0$). The negative curvatures for the λ_1 and λ_2, i.e., dominate at the BCP, the electronic charge is locally concentrated within the region inter atoms and leading to the formation of covalent or polarized bonds and is characterized by large ρBCP values, $\nabla^2\rho BCP < 0$, and $|\lambda_1|/\lambda_3 > 1$. $|\lambda_1|/\lambda_3 > 1$ On the other hand, if the positive curvature $\lambda_{3,}$ i.e., λ_3 is dominant at the BCP, the electronic density is locally concentrated in each of the atomic basins. In this case, the interaction leads to the formation of

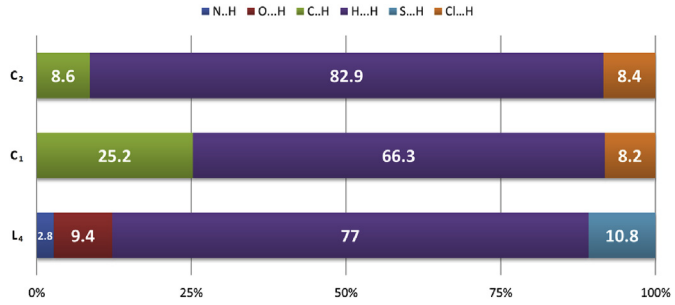

Fig. 7. The relative contributions of different intermolecular interactions to the Hirshfeld surface area in **L_4**, **C_1**, and **C_2**.

Table 5
P–N and P=O/P=S bond lengths (Å) in optimized free ligands L_n (n = 1–17) at CAM-B3LYP/def2-TZVP level of theory.

Ligand	No.	*d*(P–N)/Å		*d*(P=O/P=S)/Å	
		N^1_{chain}	N^2_{cycle}	N_{chain}	N_{cycle}
Bisphosphoramidate	L1	1.666	–	1.476	–
	L8	1.664	1.672	1.477	1.477
	L13	–	1.674	–	1.477
	L2	1.626	–	1.460	–
	L9	1.627	1.642	1.460	1.463
	L14	–	1.630	–	1.460
	L3	1.635	–	1.462	–
	L10	1.636	1.650	1.462	1.464
	L15	–	1.637	–	1.462
Bisthiophosphoramidate	L4	1.643	–	1.920	–
	L11	1.645	1.653	1.920	1.929
	L16	–	1.654	–	1.928
	L5	1.641	–	1.918	–
	L17	–	1.653	–	1.926
Bisphosphoramidate	L7	1.633	–	1.462	–
	L12	1.634	1.640	1.462	1.465
	L6	1.635	–	1.464	–

[1, 2] N_{chain} and N_{cycle} refer to two different kinds of nitrogen atoms which exist in studied ligands and investigated parameters are related to that kind of nitrogen.

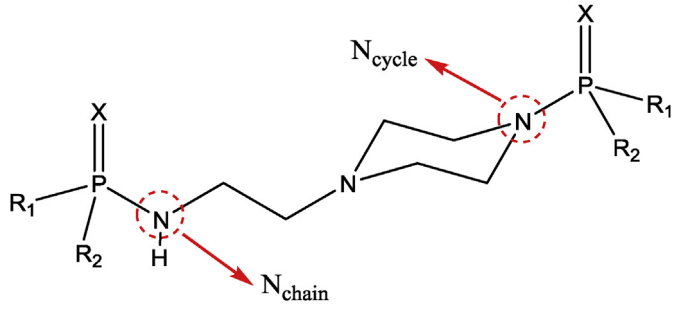

Scheme 2. Two different kinds of nitrogen in studied ligands.

highly ionic bonds, hydrogen bonds (HBs) and van der Waals interactions. It is characterized by relatively low ρBCP values, $\nabla^2\rho BCP > 0$ and $|\lambda_1|/\lambda_3 < 1$. The AIM analysis was used to determine the presence of bond critical points (BCPs) of the P=O bond in L_1 and also P=O and O···Sn^{4+} bonds in two synthesized complexes (Table 8). This comparison not only performs an authentic insight into the changes of P=O bond character before and after the complexation but also determine the nature of the O···Sn^{4+} bond.

Calculated AIM charge density (ρ), Laplacian ($\nabla^2\rho$) at the P=O BCP and also at the BCP of O···Sn^{4+} interactions are given in Table 8. Smallish values of ρ and $|\lambda_1|/\lambda_3$ at P=O BCP in the free ligand **L_1** and large values of $\nabla^2\rho$ show mostly electrostatic character for this

Table 6
Hybridization of P and O/S atoms in related P=O/P=S bonds in studied ligands at CAM-B3LYP/def2-TZVP level of theory.

No.	Hybridization			
	P in P=O/P=S		O/S in P=O/P=S	
	N_{chain}	N_{cycle}	N_{chain}	N_{cycle}
L_1	$sp^{2.43}d^{0.04}$	–	$sp^{1.60}d^{0.02}$	–
L_8	$sp^{2.45}d^{0.05}$	$sp^{2.47}d^{0.05}$	$sp^{1.60}d^{0.02}$	$sp^{1.60}d^{0.02}$
L_{13}	–	$sp^{2.47}d^{0.05}$	–	$sp^{1.58}d^{0.02}$
L_2	$sp^{1.93}d^{0.04}$	–	$sp^{1.51}d^{0.02}$	–
L_9	$sp^{1.93}d^{0.04}$	$sp^{1.89}d^{0.04}$	$sp^{1.50}d^{0.02}$	$sp^{1.48}d^{0.02}$
L_{14}	–	$sp^{1.86}d^{0.04}$	–	$sp^{1.48}d^{0.02}$
L_3	$sp^{1.96}d^{0.04}$	–	$sp^{1.55}d^{0.02}$	–
L_{10}	$sp^{1.97}d^{0.04}$	$sp^{1.96}d^{0.04}$	$sp^{1.54}d^{0.02}$	$sp^{1.55}d^{0.02}$
L_{15}	–	$sp^{2.00}d^{0.04}$	–	$sp^{1.53}d^{0.02}$
L_4	$sp^{2.47}d^{0.55}$ $sp^{7.92}d^{5.30}$	–	$sp^{4.31}d^{0.06}$ $sp^{1.00}d^{0.01}$	–
L_{11}	$sp^{2.48}d^{0.57}$ $sp^{7.87}d^{5.12}$	$sp^{2.36}d^{0.06}$ $sp^{99.99}d^{99.99}f^{1.33}$	$sp^{4.29}d^{0.06}$ $sp^{1.00}d^{0.01}$	$sp^{5.32}d^{0.09}$ $sp^{35.87}d^{0.24}$
L_{16}	–	$sp^{2.35}d^{0.06}$ $sp^{99.99}d^{99.99}f^{1.39}$	–	$sp^{5.37}d^{0.09}$ $sp^{34.15}d^{0.24}$
L_5	$sp^{2.41}d^{0.49}$ $sp^{7.62}d^{5.35}$	–	$sp^{4.11}d^{0.06}$ $sp^{1.00}d^{0.01}$	–
L_{17}	–	$sp^{2.31}d^{0.05}$ $sp^{95.99}d^{97.82}f^{1.31}$	–	$sp^{5.17}d^{0.09}$ $sp^{32.41}d^{0.24}$
L_7	$sp^{2.29}d^{0.04}$	–	$sp^{1.53}d^{0.02}$	–
L_{12}	$sp^{2.29}d^{0.04}$	$sp^{2.32}d^{0.06}$	$sp^{1.53}d^{0.02}$	$sp^{1.52}d^{0.02}$
L_6	$sp^{2.26}d^{0.04}$	–	$sp^{1.55}d^{0.02}$	–

Table 7
Wiberg bond indices (WBI) of P–N, P=O/P=S bonds and the values of $\Delta E^{(2)}$ from different atoms LP (lone pair) to BD* (antibonding) P=O and P=S in studied ligands at CAM-B3LYP/def2-TZVP level of theory.

No.	WBI				Donor-Acceptor	
	P–N		P=O/P=S		$\Delta E^{(2)}$[a]	
	N_{chain}	N_{cycle}	N_{chain}	N_{cycle}	N_{chain}	N_{cycle}
L_1	0.812	–	1.210	–	14.85	–
L_8	0.816	0.785	1.200	1.204	14.95	15.08
L_{13}	–	0.779	–	1.206	–	14.86
L_2	0.835	–	1.269	–	22.97	–
L_9	0.834	0.828	1.269	1.267	22.96	23.02
L_{14}	–	0.804	–	1.266	–	24.46
L_3	0.817	–	1.246	–	21.14	–
L_{10}	0.815	0.792	1.245	1.242	21.45	23.07
L_{15}	–	0.799	–	1.244	–	22.78
L_4	0.823	–	1.592	–	37.79	–
L_{11}	0.822	0.780	1.593	1.457	37.63	52.59
L_{16}	–	0.776	–	1.450	–	52.38
L_5	0.826	–	1.597	–	37.88	–
L_{17}	–	0.779	–	1.452	–	51.60
L_7	0.833	–	1.248	–	7.91	–
L_{12}	0.831	0.808	1.248	1.245	7.83	8.46
L_6	0.827	–	1.254	–	7.97	–

[a]The values are reported in kcal.mol^{-1}.

bond. The charge density at the P=O BCP decreases when the ligand is coordinated to the metal cation. The ρ values at the P=O BCP in ligand is 0.293 au but decreases to 0.225 and 0.217 au in **C_1** and **C_2** complexes, which is in accordance with the lengthening of the P=O bond after complexation. Analysis of the obtained bond critical points for O···Sn^{4+} interactions, suggests a closed–shell interaction and ionic character of O···Sn^{4+}. Hessian eigenvalues (λ_1, λ_2, and λ_3) of the charge density at the main BCP of the complexes are

Table 8
Calculated d(P=O)/Å bond lengths and main BCP parameters of $\mathbf{L_1}$ and related complexes at CAM-B3LYP/def2-TZVP level.

Complex	d(P=O)/Å	ρ (in au)		$\nabla^2\rho$ (in au)		$\lvert\lambda_1\rvert/\lambda_3$	
		$Sn^{4+}\cdots O$	P=O	$Sn^{4+}\cdots O$	P=O	P=O	$Sn^{4+}\cdots O$
$\mathbf{L_1}$	1.476	–	1.35	–	0.199	0.293	–
$\mathbf{C_1}$	1.491	0.045	1.18	0.201	0.214	0.205	0.162
$\mathbf{C_2}$	1.487	0.031	1.27	0.191	0.203	0.217	0.154

presented in Table 8. Very small values of ρ, $\nabla^2\rho > 0$ and $|\lambda_1|/\lambda_3 =$ (0.162 and 0.154, in $\mathbf{C_1}$ and $\mathbf{C_2}$) which is « 1 at the BCP of $O\cdots Sn^{4+}$ confirm the presence of ionic interactions. The values of $\nabla^2\rho$ at P=O BCP in both complexes are » 0 and $|\lambda_1|/\lambda_3$ «1, which attest that the P=O bond still demonstrates electrostatic nature, but with a little shift to the covalent character after the complexation.

4. Conclusions

In this study, some of the novel bisphosphoramidate and (thio) phosphoramidate derivatives ($\mathbf{L_1}$–$\mathbf{L_{12}}$), as well as two organotin(IV) complexes with diphosphoryl ligand $\mathbf{L_4}$ have been prepared and characterized by spectroscopic methods. Furthermore, the crystal structure of compound $\mathbf{L_4}$ and complexes $\mathbf{C_1}$ and $\mathbf{C_2}$ were investigated. The crystal structures of the complexes revealed that the Sn(IV) atoms are five-coordinated. The coordination geometry around tin(IV) center could be described as slightly distorted trigonal bipyramidal and confirmed the binuclear structures for the tin(IV) adducts with two trans $SnPh_3Cl/SnBu_3Cl$ linked via the bridging diphosphoryl ligand. The bidentate ligand in complexes has P=O groups in an anti conformation to each other, and the phosphorus atom showed a tetrahedral configuration as well as for ligand $\mathbf{L_4}$ in which the P=S groups are on opposite sides of the molecule. The crystal packing and the intermolecular interactions were studied. The relative contributions of different intermolecular contacts in crystal packing $\mathbf{L_4}$, $\mathbf{C_1}$ and $\mathbf{C_2}$ studied by Hirshfeld surface analysis.

Theoretical investigations on the effect of chain lengths on P=O bond strength by bond lengths, hybridization, WBI and donor-acceptor in bisphosphoramidate derivatives unanimously attested that the chain length did not make any considerable effect on P=O bond strength in both N_{chain} and N_{cycle} positions, but in the case of bisthiophosphoramidates, chain length influence on P=S bond strength is remarkable, and the bond length is larger in N_{cycle} than N_{chain}. The effect of different substituent groups in bisphosphoramidate ligands demonstrated that $\mathbf{L_1}$, $\mathbf{L_8}$, and $\mathbf{L_{13}}$ have the largest P=O and P–N bond lengths, while $\mathbf{L_2}$, $\mathbf{L_9}$, and $\mathbf{L_{14}}$ have the shortest ones. The AIM analysis was also showed ionic character for $O\cdots Sn^{4+}$ interaction in $\mathbf{C_1}$ and $\mathbf{C_2}$ synthesized complexes and mostly electrostatic character for P=O bond in free ligand $\mathbf{L_1}$, but with a little shift to the covalent character after the complexation.

Ethical statement/conflict of interest

The authors declare no conflict of interest.

Acknowledgment

Financial support of this work by Tarbiat Modares University is gratefully acknowledged.

Appendix A. Supplementary data

Supplementary data to this article can be found online at https://doi.org/10.1016/j.jorganchem.2018.10.012.

References

[1] L. Hu, X. Wu, J. Han, L. Chen, S.O. Vass, P. Browne, B.S. Hall, C. Bot, V. Gobalakrishnapillai, P.F. Searle, R.J. Knox, S.R. Wilkinson, Bioorg. Med. Chem. Lett 21 (2011) 3986–3991.
[2] Y. Jiang, L. Hu, Bioorg. Med. Chem. Lett 18 (2008) 4059–4063.
[3] Y. Jiang, R.S. DiPaola, L. Hu, Bioorg. Med. Chem. Lett 19 (2009) 2587–2590.
[4] Y. Jiang, L. Hu, Bioorg. Med. Chem. Lett 17 (2007) 517–521.
[5] Y. Mehellou, C. McGuigan, A. Brancale, J. Balzarini, Bioorg. Med. Chem. Lett 17 (2007) 3666–3669.
[6] C. McGuigan, F. Daverio, I. Nájera, J.A. Martin, K. Klumpp, D.B. Smith, Bioorg. Med. Chem. Lett 19 (2009) 3122–3124.
[7] C. McGuigan, M.R. Kelleher, P. Perrone, S. Mulready, G. Luoni, F. Daverio, S. Rajyaguru, S. LePogam, I. Nájera, J.A. Martin, K. Klumpp, D.B. Smith, Bioorg. Med. Chem. Lett 19 (2009) 4250–4254.
[8] K.D. Wing, A.H. Glickman, J.E. Casida, Pestic. Biochem. Physiol. 21 (1984) 22–30.
[9] T. Miyamoto, T. Kasagami, M. Asai, I. Yamamoto, Pestic. Biochem. Physiol. 63 (1999) 151–162.
[10] K. Gholivand, Z. Shariatinia, K. Khajeh, H. Naderimanesh, J. Enzym. Inhib. Med. Chem. 21 (2006) 31–35.
[11] J.T. Stivers, R. Nagarajan, Chem. Rev. 106 (2006) 3443–3467.
[12] V.M. Amirkhanov, V.A. Ovchynnikov, T. Glowiak, H. Kozlowski, Z. Naturforsch. B Chem. Sci. 52 (1997) 1331–1336.
[13] O.V. Moroz, V.A. Trush, I.S. Konovalova, O.V. Shishkin, Y.S. Moroz, S. Demeshko, V.M. Amirkhanov, Polyhedron 28 (2009) 1331–1335.
[14] K. Gholivand, H.M. Mahzouni, M.D. Esrafili, Dalton Trans. 41 (2012) 1597–1608.
[15] K. Gholivand, M. Rajabi, F. Molaei, H. Reza Mahzouni, S. Farshadian, J. Coord. Chem. 66 (2013) 4199–4210.
[16] K. Gholivand, R. Yaghoubi, S. Farshadian, Z. Hosseini, J. Coord. Chem. 64 (2011) 4201–4208.
[17] A.G. Davies, in: E.W. Abel, F.G.A. Stone, G. Wilkinson (Eds.), Comprehensive Organometallic Chemistry II, vol. 2, Elsevier Science Inc., Tarrytown, NY, 1995.
[18] a) P.G. Harrison, Compounds of tin: general trends, in: P.G. Harrison (Ed.), Chemistry of Tin, Chapman and Hall, New York, 1989;
b) T. Munguia, M. Lopez-Cardoso, F. Cervantes-Lee, K.H. Pannell, Inorg. Chem. 46 (2007) 1305.
[19] D. Fa`rsaiu, R. Leu, P.J. Ream, J. Chem. Soc., Perkin Trans. 2 (2001) 427.
[20] S.E. Dann, A.R.J. Genge, W. Levason, G. Reid, J. Chem. Soc. Dalton Trans. (1997) 2207.
[21] C.H. Yoder, L.A. Margolis, J.M. Horne, J. Organomet. Chem. 633 (2001) 33 (and references therein).
[22] J.M. Rivera, D. Guzman, M. Rodriguez, J.F. Lamere, K. Nakatani, R. Santillan, P.G. Lacroix, N. Farfan, J. Organomet. Chem. 691 (2006) 1722.
[23] A.G. Davies, Organotin Chemistry, second ed., Wiley-VCH, Weinheim, 2004, p. 383.
[24] M. Gielen, M. Biesemans, R. Willem, Appl. Organomet. Chem. 19 (2005) 440.
[25] A.J. Crowe, P.J. Smith, G. Atassi, Chem. Biol. Interact. 32 (1980) 171.
[26] A.J. Crowe, P.J. Smith, G. Atassi, Inorg. Chim. Acta. 93 (1984) 179.
[27] A.K. Saxena, F. Huber, Coord. Chem. Rev. 95 (1989) 109.
[28] H.I. Beltran, C. Damian-Zea, S. Hernandez-Ortega, A. Nieto-Camacho, M.T. Ramiraz-Apan, Inorg. Biochem. 101 (2007) 1070.
[29] T.A.K. Al-Allaf, L.J. Rashan, A. Stelzner, D.R. Powell, Appl. Organomet. Chem. 17 (2003) 891.
[30] M. Nath, R. Yadav, M. Gielen, H. Dalil, D. de Vos, G. Eng, Appl. Organomet. Chem. 11 (1997) 727.
[31] L. Tian, Z. Shang, X. Zheng, Y. Sun, Y. Yul, B. Qian, X. Liu, Appl. Organomet. Chem. 20 (2006) 74.
[32] L.S. Zamudio-Rivera, R. George-Tellez, G. Lopez-Mendoza, A. Morales-Pacheco, E. Flores, H. Hopfl, V. Barba, F.J. Fernandez, N. Cabirol, H.I. Beltran, Inorg. Chem. 44 (2005) 5370.
[33] H.L. Singh, A.K. Varshney, Appl. Organomet. Chem. 15 (2001) 762.
[34] T.S. Basu Baul, Appl. Organomet. Chem. 22 (2008) 195.
[35] A. Ruzicka, L. Dostal, R. Jambor, V. Buchta, J. Brus, I. Cisarova, M. Holcapek, J. Holecek, Appl. Organomet. Chem. 16 (2002) 315.
[36] D.J. Darensbourg, P. Ganguly, D. Billodeaux, Macromolecules 38 (2005) 5406.
[37] H. Reyes, C. Garcia, N. Farfan, R. Santillan, P.G. Lacroix, C. Lepetit, K. Nakatani, J. Organomet. Chem. 689 (2004) 2303.
[38] J. Lorberth, S. Wocadlo, W. Massa, N.S. Yashina, E.V. Grigoriev, V.S. Petrosyan, J. Organomer. Chem. 480 (1994) 163 (and references cited therein).
[39] M. Gielen, Appl. Organomet. Chem. 16 (2002) 481.
[40] A.G. Davies, M. Gielen, K.H. Pannell, E.R.T. Tiekink (Eds.), Tin Chemistry: Fundamen Tal, Frontiers, and Application, John Wiley and Sons, New York, 2008.
[41] M. Gielen, E.R.T. Tiekink, in: M. Gielen, E.R.T. Tiekink (Eds.), Metallotherapeutic Drugs and Metal-based Diagnostic Agents, Johan Willey and Sons, Chichester, 2005, p. 421.
[42] E.V. Grigoriev, N.S. Yashina, A.A. Prischenko, M.V. Livantsov, V.S. Petrosyan, W. Massa, K. Harms, S. Wocadlo, L. Pellerito, Appl. Organomet. Chem. 9 (1995) 11.
[43] E.V. Grigorev, N.S. Yashina, A.A. Prischenko, M.V. Livantsov, V.S. Petrosyan, L. Pellerito, M.J. Schafer, Appl. Organomet. Chem. 7 (1993) 353.
[44] K. Gholivand, A. Madani Alizadehgan, A. Anaraki Firooz, K. Khajeh, H. Naderi-

Manesh, H. Bijanzadeh J, Enzyme Inhib. Med. Chem 21 (1) (2006) 105–111.
[45] A.V. kirsanov, G.I. Derkach, zhur, obshchei khim. 26 (1956) (1956) 2082.
[46] a) K. Gholivand, A. Gholami, A.A.V. Ebrahimi, S.T. Abolghasemi, F.T. Fadaei, K.J. Schenk, M.D. Esrafili, RSC Adv. 5 (2015) 17482–17492;
b) M. Pourayoubi, P. Zargaran, Acta Crystallogr. E: Struct. Rep. Online 66 (2010), 03273;
c) Khodayar Gholivand, Mahdieh Hosseini, A. Ali, Ebrahimi valmoozi and kaveh farshadfar, CrystEngComm 19 (2017) 2536–2548;
d) Khodayar Gholivand, Ali Asghar Ebrahimi Valmoozi, Mahyar Bonsaii, J. Agric. Food Chem. 62 (2014), 5761–577.
[47] G. Sheldrick, Acta Crystallogr. A 64 (2008) 112.
[48] G.M. Sheldrick, Acta Crystallographica. Section C, Structural Chemistry 71 (2015) 3.
[49] C.F. Macrae, I.J. Bruno, J.A. Chisholm, P.R. Edgington, P. McCabe, E. Pidcock, L. Rodriguez-Monge, R. Taylor, J. van de Streek, P.A. Wood, J. Appl. Crystallogr. 41 (2008) 466–470.
[50] M.J. Frisch, G.W. Trucks, H.B. Schlegel, G.E. Scuseria, M.A. Robb, J.R. Cheeseman, J.A.J. Montgomery, T. Vreven, K.N. Kudin, J.C. Burant, J.M. Millam, S.S. Iyengar, J. Tomasi, V. Barone, B. Mennucci, M. Cossi, G. Scalmani, N. Rega, G.A. Petersson, H. Nakatsuji, M. Hada, M. Ehara, K. Toyota, R. Fukuda, J. Hasegawa, M. Ishida, T. Nakajima, Y. Honda, O. Kitao, H. Nakai, M. Klene, X. Li, J.E. Knox, H.P. Hratchian, J.B. Cross, C. Adamo, J. Jaramillo, R. Gomperts, R.E. Stratmann, O. Yazyev, A.J. Austin, R. Cammi, C. Pomelli, J.W. Ochterski, P.Y. Ayala, K. Morokuma, G.A. Voth, P. Salvador, J.J. Dannenberg, V.G. Zakrzewski, S. Dapprich, A.D. Daniels, M.C. Strain, O. Farkas, D.K. Malick, A.D. Rabuck, K. Raghavachari, J.B. Foresman, J.V. Ortiz, Q. Cui, A.G. Baboul, S. Clifford, J. Cioslowski, B.B. Stefanov, G. Liu, A. Liashenko, P. Piskorz, I. Komaromi, R.L. Martin, D.J. Fox, T. Keith, M.A. Al- Laham, C.Y. Peng, A. Nanayakkara, M. Challacombe, P.M.W. Gill, B. Johnson, W. Chen, M.W. Wong, C. Gonzalez, J.A. Pople, Gaussian 03, Revision C.01, Gaussian, Inc., Pittsburgh, 2003.
[51] Y. Tawada, T. Tsuneda, S. Yanagisawa, T. Yanai, K. Hirao, J. Chem. Phys. 120 (2004) 8425.
[52] F. Weigend, R. Ahlrichs, Phys. Chem. Chem. Phys. 7 (2005) 3297.
[53] F. Biegler-König, J. Schönbohm, D. Bayles, AIM2000-A Program to Analyze and Visualize Atoms, University of Applied Science, Bielefeld, 2001.
[54] A.E. Reed, L.A. Curtiss, F. Weinhold, Chem. Rev. 88 (6) (1988) 899–926.
[55] A. Bondi, J. Phys. Chem. 68 (1964) 441.
[56] P.J. Smith (Ed.), Chemistry of Tin, second ed., Blackie, London, 1998.
[57] a) F.H. Allen, S.A. Bellard, M.D. Brice, B.A. Cartwright, A. Doubleday, H. Higgs, T. Hummelink, B.G. Hummelink-Peters, O. Kennard, W.D.S. Motherwell, J.R. Rogers, D.G. Watson, Acta Crystallogr. B 35 (1979) 2331;
b) A.R. Narga, M. Schuermann, C. Silvestru, J. Organomet. Chem. 623 (2001) 161;
c) P.J. Smith (Ed.), Chemistry of Tin, second ed., Blackie, London, 1998.
[58] a) J.S. Casas, A. Castineriros, E.G. Martines, A.S. Gonzales, A. Sanches, J. Sordo, Polyhedron 16 (1997) 795;
b) M. Hill, M.F. Mahon, K.C. Molloy, J. Chem. Soc. Dalton Trans. (1996) 1857;
c) S. Bhandari, M.F. Mahon, K.C. Molloy, J. Chem. Soc. Dalton Trans. (1999) 1951;
d) N.W. Alcock, J.F. Sawyer, J. Chem. Soc., Dalton Trans. 1090 (1977).
[59] A. Bondi, J. Phys. Chem. 68 (1964) 441.
[60] D.E.C. Corbridge, Phosphorus: an Outline of its Chemistry, Biochemistry and Technology, fifth ed., Elsevier, Amsterdam, 1995.
[61] M.A. Spackman, P.G. Byrom, Chem. Phys. Lett. 267 (1997) 215.
[62] J.J. McKinnon, M.A. Spackman, A.S. Mitchell, Acta Crystallogr. Sect. B Struct. Sci. 60 (2004) 627.
[63] M.A. Spackman, J.J. McKinnon, CrystEngComm 4 (2002) 378.
[64] S.K. Wolff, D.J. Grimwood, J.J. McKinnon, M.J. Turner, D. Jayatilaka, M.A. Spackman, CrystalExplorer 3.0, University of Western Australia, Perth, Australia, 2012.
[65] I. Mayer, On bond orders and valences in the ab initio quantum chemical theory, Int. J. Quant. Chem. 29 (1) (1986) 73–84.